CATalytic – Post Processor (CAT-PP): A new methodology for the CFD-based simulation of highly diluted reactive heterogeneous systems

Michele Corbetta [a], Flavio Manenti [a,*], Carlo Giorgio Visconti [b]

[a] *Politecnico di Milano, Dipartimento di Chimica, Materiali e Ingegneria Chimica "Giulio Natta", Piazza Leonardo da Vinci, 32, 20133 Milano, Italy*
[b] *Politecnico di Milano, Dipartimento di Energia, Piazza Leonardo da Vinci, 32, 20133 Milano, Italy*

Article history:
Received 14 May 2013
Received in revised form 7 August 2013
Accepted 22 August 2013
Available online xxx

1. Introduction

One of the pre-requisites of lab-scale reactors is the ideal fluid-dynamic, which could be described either through a plug-flow model or assuming a perfectly mixed environment (Manenti, Cieri, Restelli, & Bozzano, 2013; Visconti et al., 2011). Such a pre-requisite is usually satisfied by working in thin tubular reactors or in continuous stirred tank units, and carefully selecting the reacting mixture space velocity and the stirring rate. Industrialization or miniaturization of lab-scale reactors, however, often entails the introduction of non-idealities in the reactor flow field. For example, the adoption of large stirred reactors usually implies the existence of dead-zones, where the local concentrations of reactants and products differ from those in other parts of the reactor. In industrial multi-tubular reactors, instead, the feed can be non-uniformly split among the different tubes due to maldistribution problems.

In the last decade, researchers in the field of heterogeneous catalysis have devoted a lot of attention to the characterization of catalysts *operando* conditions. In particular, the adoption of spectroscopic techniques to look at the catalyst surface when it is working at the actual process conditions has strongly contributed to the comprehension of the reason why a given material is a good or a bad catalyst for this or that reaction. For example, the adoption of *operando* FTIR allowed to definitely point out the role of nitrites and nitrates as surface intermediates in the lean-NO_x trap (Lietti et al., 2012; Nova et al., 2004), a well-known process for the abatement of the NO_x emissions from internal combustion engines. Implementation of *operando* spectroscopic techniques often requires to employ catalytic reactors with special geometries, which are not only very different from those adopted in industrial operations, but which are also very different from conventional ideal lab-scale reactors: in such miniaturized reactors it is not uncommon that the flow path strongly deviates from the desired ideal fluid-dynamics. For instance, some authors investigated the non-idealities (Carias-Henriquez, Pietrzyk, & Dujardin, 2013; Meunier, 2010) that are introduced because of the geometrical constraints necessary for the

* Corresponding author. Tel.: +39 02 2399 3273; fax: +39 02 7063 8173.
E-mail address: flavio.manenti@polimi.it (F. Manenti).

Nomenclature

t	time (s)
T	reaction temperature (K)
R	ideal gas constant (J/mol/K)
x_i	molar fraction of the i-th gaseous species
θ_j	surface coverage of the j-th adspecies
ρ_i^{C}	massive concentration of i-th gaseous species on cell C centroid (kg/m^3)
ρ_i^{f}	massive concentration of i-th gaseous species on face f centroid (kg/m^3)
ΔV_{cell}	computational cell volume (m^3)
$\mathbf{v}_{\mathrm{f}}$	mesh face velocity (m/s)
A_{f}	face area (m^2)
$\mathbf{n}_{\mathrm{f}}$	face normal vector
N_{FACES}	number of faces of a computational cell
F_{int}	number of internal faces of a computational cell
F_{ext}	number of boundary faces (on solid-wall) of a computational cell
$\boldsymbol{N}_i$	mass flux (kg/s)
R_i	reaction source term (mol/m^3/s)
MW_i	molar weight (g/mol)
V_{cat}	catalyst overall volume (m^3)
A_{cat}	catalyst geometrical external area (m^2)
Ω_{site}	active site concentration (load) (mol/m^3)
σ_j	coordination number of j-th adspecies

IR transmission across a thin catalyst pellet (≈0.1 mm) in *operando* FTIR cells, and the restrictions in micro-reactor design due to the small length scales.

The mathematical modeling of non-ideal catalytic reactors would require reactive computational fluid-dynamic (CFD) simulations. Deutschmann (2001) developed models and tools for the numerical simulation of heterogeneous reactive flows, in which all physical and chemical processes are described as detailed as possible. However, this approach requires massive computational efforts, which arise from the wide time and space scales, as well as from the presence of reactive species both in the gas phase and adsorbed on the active sites. This may result in the practical impossibility to simulate those reactors within an acceptable computational time.

In order to simplify the computational burden, different hypothesis can be introduced. For example Kolaczkowski, Chao, Awdry, and Smith (2007) approached the simulation of an isolated spherical pellet by means of the commercial code ANSYS Fluent, adopting a standard Arrhenius expression for the definition of the heterogeneous reaction rates, thus neglecting the effect of the surface coverage on kinetics. Moreover they do not solve any equation for the chemical evolution of the adsorbed species on the active catalytic surface. Very recently Maestri and Cuoci (2013) proposed a different methodology for the coupling of CFD with detailed microkinetic models for heterogeneous reactions. They highlighted the impossibility to efficiently apply conventional CFD methods to this kind of stiff and non-linear problems because these methods are based on segregated algorithms. They proposed a technique based on the operator-splitting approach which can reduces the numerical difficulty of fully coupled methods.

Another strategy to simplify the problem is here proposed in relation to the specific case, which is typical of most of the processes of environmental catalysis (Centi, Ciambelli, Perathoner, & Russo, 2002), of reactors operating with highly diluted process streams, where reactants and products have concentrations of hundreds or thousands of parts per million. In those units fluid dynamic is not affected by the kinetics of the reactive system. In this work a new methodology is presented, named "CATalytic – Post Processor (CAT-PP)", able to effectively simulate with a fully coupled CFD approach these highly diluted reactive heterogeneous systems. According to CAT-PP approach, the reactor fluid-dynamics is solved through a conventional non-reactive CFD calculation performed with commercial software; then, through the adoption of an appropriate post-processor, the results of the CFD simulation (i.e. the flow-field computed under non-reactive conditions) is used to solve transport equations for the species present in the system within a dedicated C++ code. This approach allows both to reduce the computational costs and to exploit very efficient differential solvers for stiff problems (Buzzi-Ferraris & Manenti, 2012; Manenti, 2011). Moreover, by adopting this approach, the simulator will be also operable on commercial PCs, relaxing the essential need for a cluster workstation (Corbetta et al., 2013).

The CAT-PP is then applied to the simulation of an *operando* FTIR reactor-cell, loaded with a Pt-BaO/γ-Al_2O_3 catalyst for DeNO_x processes. This latter is a relevant catalytic process proposed in the '90s by Toyota, which is receiving a growing attention in the last years as a technology applicable to small passenger cars to fulfill the new tight regulations on the NO_x emissions from internal combustion engines, such as the Euro 6 (European Parliament, 2007). A few authors faced indeed the modeling of LNT systems with a reactive CFD approach, but this required important simplifications. Benjamin and Roberts (2007), for example, proposed the simulation of a LNT monolith with a porous medium approach, which drastically simplifies the description of the flow field inside the catalyst; moreover they used a simplified kinetic scheme, involving reaction rates which only depends on the gas phase composition. On the other hand, Stepanek, Koci, Marek, and Kubicek (2012) developed a pseudo-3D CFD approach, based on multiple 1D simulations of a single LNT monolith channel.

In this work, a more detailed, and at the same time general, approach has been followed and the Navier–Stokes equations have been solved in the actual 3D geometry of the reactor exploiting the full potential of the new approach. A detailed surface kinetics (Visconti et al., 2013) has been implemented in the model. This work has two main implications. On a more fundamental level, it demonstrates the power of the CAT-PP approach herein proposed, which allows to perform simulations of complex catalytic reactors characterized by non-ideal flow fields, in which multi-step reactions take place. On a more applied level, it allows to assess the extent of the non-idealities of the simulated *operando* FTIR reaction cell, which is commercially available and is used by many research groups worldwide. Such a result is extremely relevant especially for all those who want to use the cell to collect quantitative information, since it will allow to verify whether the cell may be described as an ideal reactor or not. This latter hypothesis has been done for example by Visconti et al. (2013) to develop the first comprehensive and physically consistent spectrokinetic model for the NO_x storage over a representative LNT catalyst on the basis of a set of transient surface and gas-phase experimental data (Lietti et al., 2012) collected in such a cell.

2. CATalytic – Post Processor (CAT-PP)

A numerical tool is built-up ex novo in order to simulate with a CFD approach catalytic reactors where diluted streams are converted. The main hypothesis underlying the following procedure is related to the possibility to decouple reactor fluid dynamic and process kinetics, which is theoretically justified considering that the conversion of diluted streams does not affect the reactor fluid dynamic.

According to the proposed approach, which is sketched in Fig. 1, a non-reactive CFD simulation is firstly performed with a

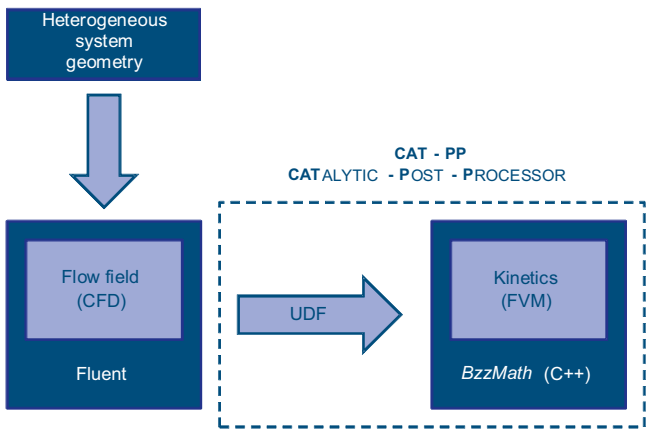

Fig. 1. Proposed approach (UDF stands for user-defined-function and FVM for Finite-Volume-Method).

commercial software (ANSYS Fluent in our case), in which the feed stream is composed by an inert gas (e.g., argon, nitrogen) with the same flow rate and temperature of the actual reacting mixture (laminar, stationary, and monocomponent model). In a second phase the flow field is exported from the commercial code by means of a user-defined-function (UDF). In a third and last phase exported data are introduced in a C++ code, which solves the transport equations, taking into account both the chemical kinetics and the reactor fluid dynamics.

2.1. Non-reactive CFD modeling

It is assumed that the chemical evolution of the system does not affect the flow field inside the reactor because of the following considerations. First of all modeled reacting flows, highly diluted, are characterized by the presence of small concentration of reactants and products, and the inert components usually account for more than 90 mol%. Moreover the temperature field inside the cell is not significantly perturbed by the extremely low reaction duty. Finally, a steady-state flow field is assumed due to the hydrodynamic time scale, which is rather fast if compared to the typical characteristic time of chemical kinetics.

2.2. User-defined-function (UDF)

The UDF was built up by using the fluent looping, data access and connectivity macros (ANSYS, 2009). Cell and face variables were exported in a database file, while the interconnections between different computational grid elements were stored in a different file, whose structure is reported in Fig. 2.

This file has got a recurring structure for each computational cell. A block of $N_{\text{faces}} + 1$ rows is reserved for each cell. The first row contains information about the cell zone and thread, as well as the number of faces. The next N_{faces} rows are reserved for each face of the actual cell, and they provide information about face zones and threads, as well as the identification of the adjacent cell with respect to the face considered. The UDF code is reported in the Appendix for sake of completeness.

2.3. Reactor modeling

According to the proposed approach, the flow field is obtained with a commercial CFD code, while the chemical evolution of the system is found solving the equations shown in the following sections.

2.3.1. Model equations

2.3.1.1. Gaseous species transport equations. The gas phase evolution is obtained by solving the gas species transport equations (Eq. (1)) with the corresponding initial conditions (IC, Eq. (2)) and boundary conditions (BC, Eqs. (3)–(6)) in each control volume of the computational grid, according to the Finite-Volume-Method (FVM).

$$\frac{d\rho_i^C}{dt}\Delta V_{\text{cell}} = -\sum_f^{F\,\text{int}} \rho_{i,f}\vec{v_f}\cdot\vec{n}_f A_f + \sum_f^{F\,\text{ext}} R_i(\overrightarrow{C^{CS}}, \overrightarrow{\theta^{CS}}) MW_i V_{\text{cat}} \frac{A_f}{A_{\text{cat}}} \quad (1)$$

IC:

$$\rho_i^C(t=0,\ \vec{c}\in\wp_{\text{gas}}) = \rho_{i,0} \quad (2)$$

BC (Fig. 3):

$$\rho_i^C(t>0,\ \vec{c}\in\partial\wp_{\text{inlet}}) = \rho_{i,IN} \quad (3)$$

$$\nabla\rho_i^C(t>0,\ \vec{c}\in\partial\wp_{\text{outlet}}) = 0 \quad (4)$$

$$-\vec{n}_f\cdot\vec{N}_i^c(t>0,\ \vec{c}\in\partial\wp_{\text{fluid-wall}}) = 0 \quad (5)$$

$$-\vec{n}_f\cdot\vec{N}_i^c(t>0,\ \vec{c}\in\partial\wp_{\text{solid-wall}}) = R_i MW_i V_{CAT}\frac{A_f}{A_{CAT}} \quad (6)$$

In Eqs. (1)–(6), subscript i refers to gas phase reactants and products, while superscript c refers to gas phase cell threads. In Eq. (1) the accumulation term is equalized to the summation of the convective and reactive fluxes. The reactive term is computed only when a control volume has a face adjacent to the catalytic geometrical surface (F_{ext}), while the other terms are considered for internal faces (F_{int}). Face variables, denoted by the subscript f, are computed with a First Order Upwind Scheme. If Peclet's number, defined as shown in Eq. (7), is significantly greater than 1 (as it happens for the LNT case study shown in Section 3, it is possible to neglect the diffusion term.

$$Pe_{i,LNT} = \frac{vL}{\wp_{i,\text{mix}}} \approx 20 \quad (7)$$

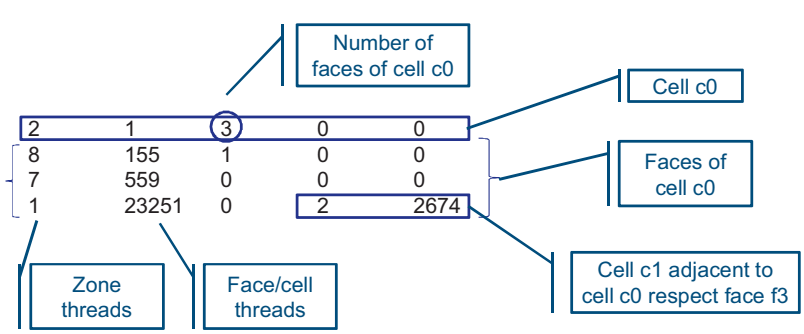

Fig. 2. Layout of the file "ExportedConnectivityVariables.txt".

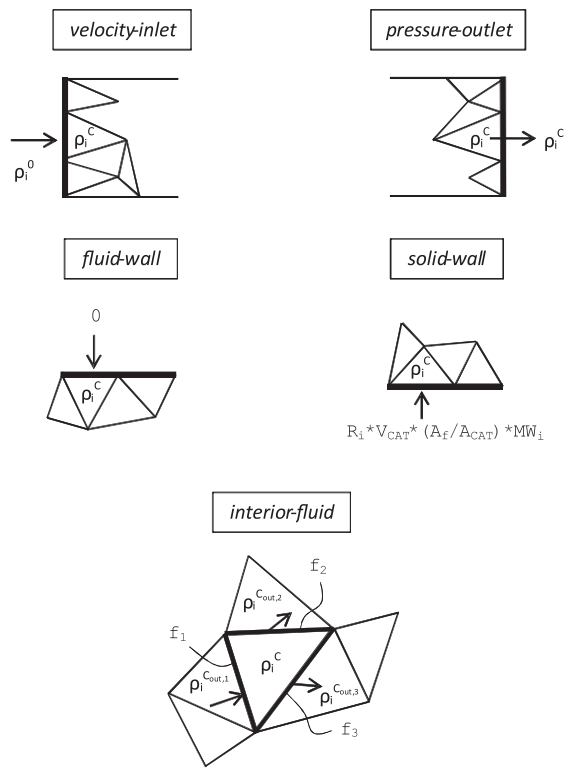

Fig. 3. Boundary conditions.

Boundary conditions involve the imposition of inlet profiles (Eq. (3)), the Neumann condition of zero-gradient on outflows (Eq. (4)), the reactive flux on active surfaces (Eq. (6)) and the zero-flux on inert walls (Eq. (5)), as displayed in Fig. 3.

2.3.1.2. Adspecies material balances. The evolution of the adsorbed species was obtained solving the corresponding material balances (Eq. (8)), according to the Mean Field Approximation (MFA) (Deutschmann, 2001).

$$\Omega_{\text{site}} \frac{d\theta_j^{Cs}}{dt} = \sigma_j R_j(\overrightarrow{C^{Cs}}, \overrightarrow{\theta^{Cs}}) \tag{8}$$

IC:

$$\theta_j^{Cs}(t=0) = \theta_{j,0}^{Cs} \tag{9}$$

In Eqs. (8) and (9) subscript j refers to adspecies, while superscript Cs refers to cells adjacent to the solid wall.

The evolution of the free active sites is obtained by solving the site balances (Eq. (10)):

$$\theta_{\text{free-site}}^{Cs}(t) = 1 - \sum_{j=\text{adspecies}} \theta_j^{Cs}(t) \tag{10}$$

2.3.2. Numerical methods

The resulting large-scale, sparse and stiff ODE system has been implemented and solved in C++, making use of the solvers of BzzMath numerical library[1] (Buzzi-Ferraris & Manenti, 2012). Due to the nature of the problem, the resulting Jacobian matrix is indeed diagonally dominant and sparse. Accordingly, the BzzOdeSparseStiff class, which allows to create an object initialized with a constructor able to acquire the Jacobian matrix structure, has been adopted. In this way it is possible to save computational resources and to exploit the stiff solvers belonging to BzzMath library, in particular those based on the Gear multivalue family (Durand, Manenti, Bandoni, Diaz, & Buzzi-Ferraris, 2012; Manenti, 2011). These solvers are much more effective than alternative algorithms, which instead require very small integration steps to solve such kinds of problems: in this solver, in fact, the integration step is progressively changed according to the local error, and the algorithm order is selected as the optimal one in relation to the actual integration step size. In order to cope with algorithm stability, it is mandatory to adopt implicit methods. As a consequence it is necessary to solve nonlinear systems in every integration step with a Newton's method trough the factorization of the Jacobian matrix.

[1] http://homes.chem.polimi.it/gbuzzi/.

3. Case-study: dynamic simulation of an *operando* FTIR cell used to study the NO_x storage on a LNT catalyst

In the following sections, the dynamic simulation of an operando FTIR cell used to study the NO_x storage on a LNT catalyst will be reported. Details on the process kinetics (Section 3.1), on the reactor geometry (Section 3.2), on the non-reactive CFD simulations (Section 3.3) and on the reactive simulations (Section 3.4) will be given.

3.1. Reaction pathway and kinetic scheme

The kinetics of the process has been described through the detailed kinetic model proposed by Visconti et al. (2013), which involves both gas phase (oxygen, nitrogen monoxide, nitrogen dioxide) and adsorbed species (nitrites, nitrates and atomic oxygen). According to the adopted kinetic mechanism, NO_x accumulation can follow two different paths, namely the nitrite route and the nitrate route. Nitrite route proceeds with a stepwise oxidation mechanism occurring at Pt–Ba couples and leads to the formation of nitrite adspecies (reaction S3) from gas phase NO. Nitrate route involves instead the NO_2 formed by NO oxidation (reaction S2) and brings to the formation of adsorbed nitrates (reaction S4). Nitrites can be also converted into nitrates by gas phase NO_2 (reaction S5) (Lietti et al., 2012; Nova et al., 2004).

$$2\text{Pt} + O_2 \leftrightarrow 2\text{Pt-O} \tag{S1}$$

$$\text{Pt-O} + \text{NO} \leftrightarrow \text{Pt} + NO_2 \tag{S2}$$

$$\text{Pt-O} + O^{2-} + 2\text{NO} \rightarrow \text{Pt} + 2NO_2^{-} \tag{S3}$$

$$2NO_2 + O^{2-} \rightarrow NO_2^{-} + NO_3^{-} \tag{S4}$$

$$NO_2 + NO_2^{-} \leftrightarrow \text{NO} + NO_3^{-} \tag{S5}$$

Rate expressions shown in Eqs. (11)–(15) were associated to reactive steps S1–S5 (Visconti et al., 2013):

$$r_{S1} = k_{S1d} x_{O_2} \theta_{\text{Pt}}^{\ 2} - k_{S1i} \theta_{\text{Pt-O}}^{\ 2} \tag{11}$$

$$r_{S2} = k_{S2d} x_{\text{NO}} \theta_{\text{Pt-O}} - k_{S2i} x_{NO_2} \theta_{\text{Pt}} \tag{12}$$

$$r_{S3} = k_{S3d} x_{\text{NO}} \theta_{\text{Pt-O}} \theta_{O_2^-} \tag{13}$$

$$r_{S4} = k_{S4d} x_{NO_2}^{\ 2} \theta_{O_2^-} \tag{14}$$

$$r_{S5} = k_{S5d} x_{NO_2} \theta_{NO_2^-} - k_{S5i} x_{\text{NO}} \theta_{NO_3^-} \tag{15}$$

More details on the kinetic expressions can be found elsewhere (Visconti et al., 2013).

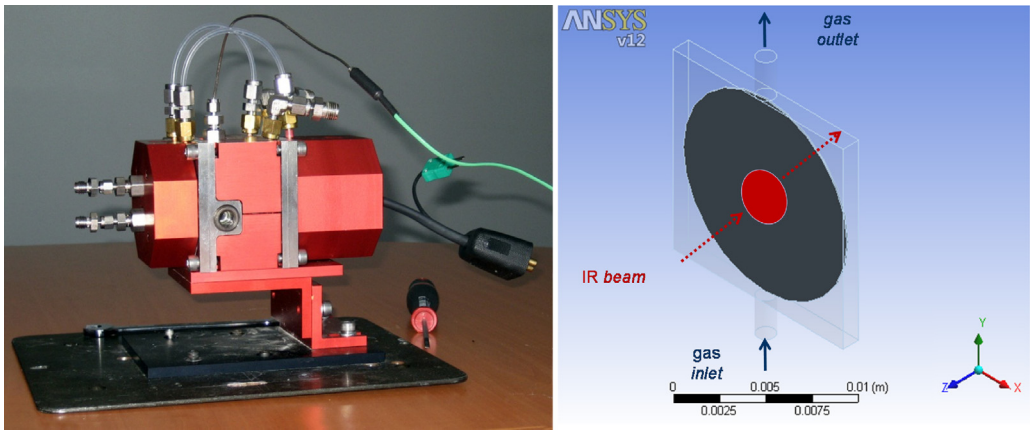

Fig. 4. AABSPEC #CX reactor-cell and schematic geometry of the sample holder with the catalytic pellet.

3.2. Reactor geometry

Experimental data were collected by the use of the AABSPEC #CX FT-IR spectroscopic reactor-cell shown in Fig. 4 (Visconti et al., 2013).

This cell was loaded with a thin cylindrical-shaped catalytic pellet, made of Pt-Ba/γ-Al_2O_3. The cell was fed with an argon stream, which was enriched of $NO + O_2$ (1000 ppm + 3% v/v) at the initial time. The temporal evolution of both the adspecies and the gaseous species was monitored. Adspecies within the IR-beam circular zone (D_{IR} = 4 mm) were analyzed with the FT-IR spectrometer, while the gas phase at the outlet of the cell was analyzed with mass spectrometer and ozone chemiluminescence.

3.3. Non-reactive CFD simulations

The reactive chamber was reconstructed in the ANSYS environment as a parallelepiped 1.2 mm wide and with a square base of 13 mm length. The catalytic pellet was reproduced by a 0.1 mm thin cylindrical pellet with a diameter of 13 mm. Fig. 5 reports the mesh adopted in the simulation (≈10,000 cells) that covers a quarter of the entire geometry, exploiting two axial symmetries.

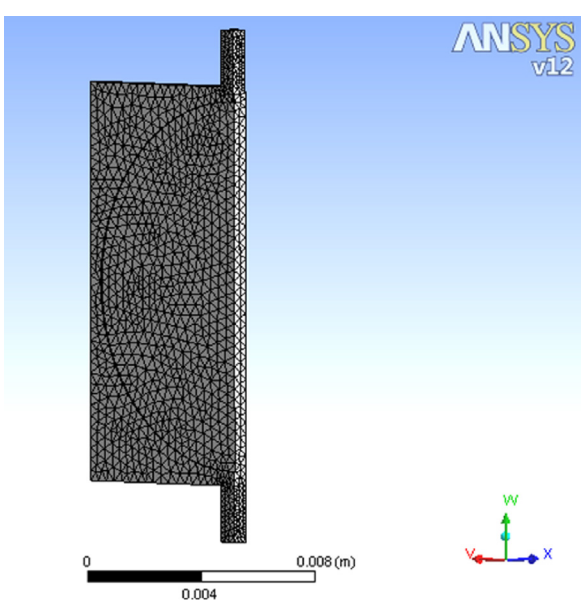

Fig. 5. mesh of the fluid domain.

Boundary conditions were defined at the inlet, outlet, fluid-wall and solid-wall. At the inlet a velocity-inlet boundary-type was imposed, with a velocity of 0.9 m/s, in agreement with an argon inlet volumetric flowrate of 25 Ncc/min. At the outlet a pressure-outlet boundary-type was selected, with a pressure of 0 barg. Finally at fluid-wall and solid-wall boundaries a non-slip condition was imposed. These last two wall boundaries were considered as perfect walls, in fact the roughness of the solid pellet is negligible after the pre-processing of the catalytic powder. The gas stream is fed from the bottom inlet capillary, crosses the sample-holder, licking the solid-wall, and finally exits from the top outlet capillary.

Simulation results are reported in Fig. 6 for the whole geometry, in order to better highlight the flow pattern. After the inlet zone, the gas flow proceeds with a uniform front in the axial direction, until it reaches the outlet zone. The contour plots on the cross-sections of the chamber show that the axial velocity is bigger in the central portion, while the streamlines of the velocity magnitude provide a qualitative idea of the general flow pattern across the reactor. The system is thus quite ideal in the central portion of the cell and behaves similarly to a plug-flow reactor. Nevertheless non-idealities are introduced by the fact that the catalytic pellet has a circular geometry, while the sample holder is square.

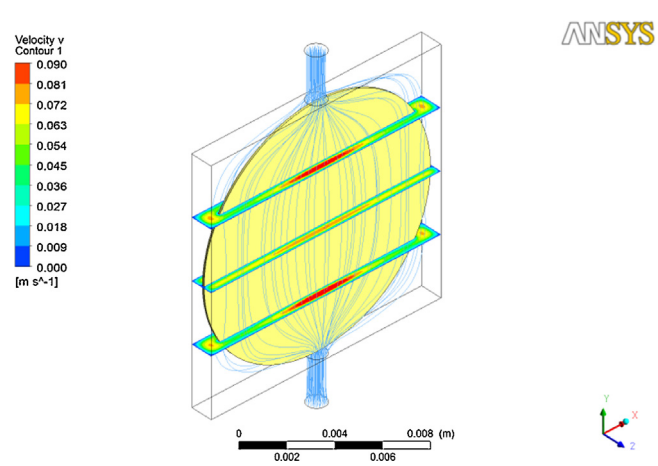

Fig. 6. CFD simulation: steamlines of the velocity magnitude and axial velocity contours on the cross-section central planes. (The legend refers to the axial velocity contours.)

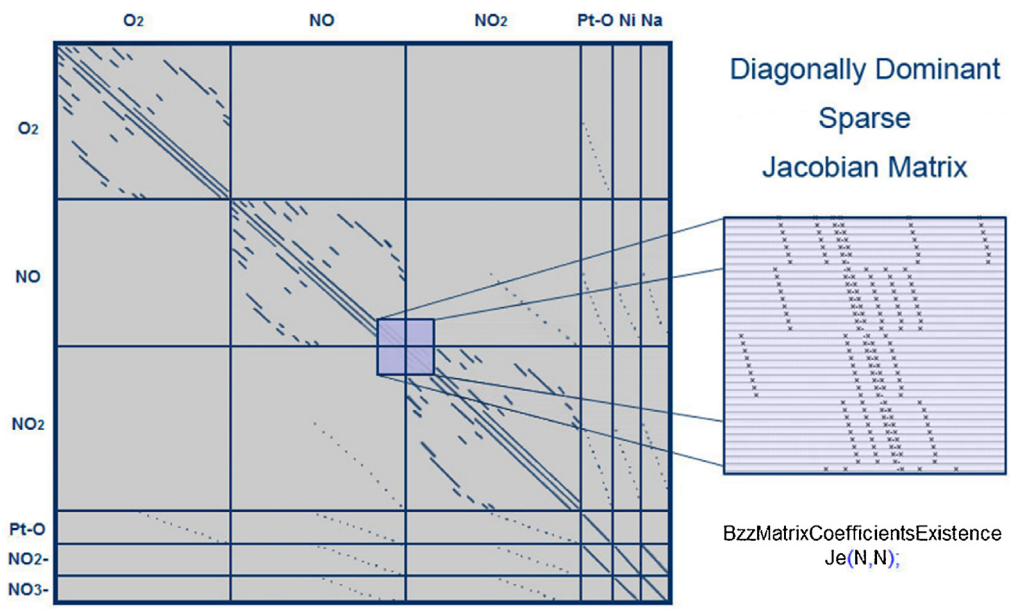

Fig. 7. Jacobian matrix structure.

3.4. Reactive simulations

The chemical evolution of the system was obtained by solving the following Eqs. (16)–(19) with IC (20)–(22) and BC (23)–(28).

$$\frac{d\rho_i^C}{dt}\Delta V_{\text{cell}} = -\sum_f^{F\,\text{int}} \rho_{i,f}\vec{v_f}\cdot\vec{n}_f A_f + \sum_f^{F\,\text{ext}} R_i(\overrightarrow{C^{Cs}}, \overrightarrow{\theta^{Cs}}) MW_i V_{\text{cat}} \frac{A_f}{A_{\text{cat}}} \quad (16)$$

$$\Omega_{\text{site}}\frac{d\theta_j^{Cs}}{dt} = \sigma_j R_j(\overrightarrow{C^{Cs}}, \overrightarrow{\theta^{Cs}}) \quad (17)$$

$$\theta_{Pt}^{Cs} = 1 - \theta_{Pt-0}^{Cs} \quad (18)$$

$$\theta_{\text{Ba0}}^{Cs} = 1 - \theta_{\text{Nitrite}}^{Cs} - q_{\text{Nitrate}}^{Cs} \quad (19)$$

IC:

$$\rho_{i=\text{O}_2}^C(t=0, \vec{c}\in\wp_{\text{gas}}) = \frac{0.03\cdot P\cdot MW_{\text{O}_2}}{RT} \quad (20)$$

$$\rho_{i\neq\text{O}_2}^C(t=0, \vec{c}\in\wp_{\text{gas}}) = 0 \quad (21)$$

$$\theta_j^{Cs}(t=0) = 0 \quad (22)$$

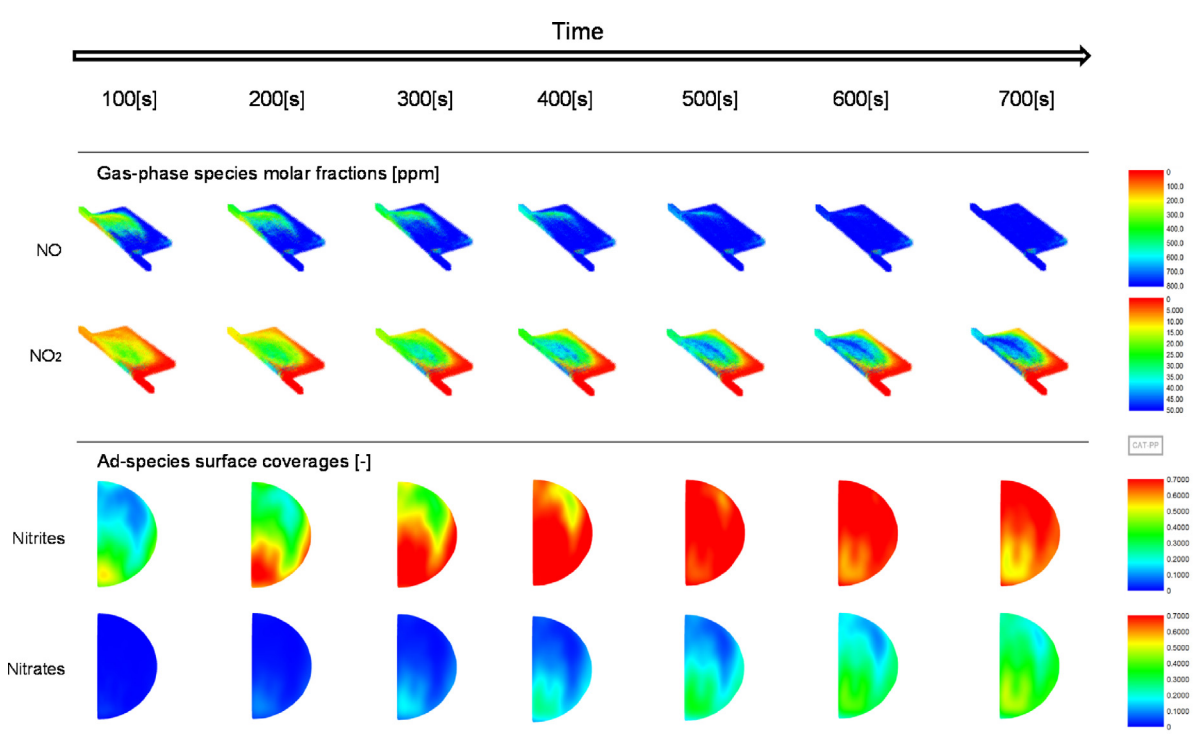

Fig. 8. Gas phase composition fields and space-time evolution of the surface coverage @ $T = 250\,^{\circ}\text{C}$.

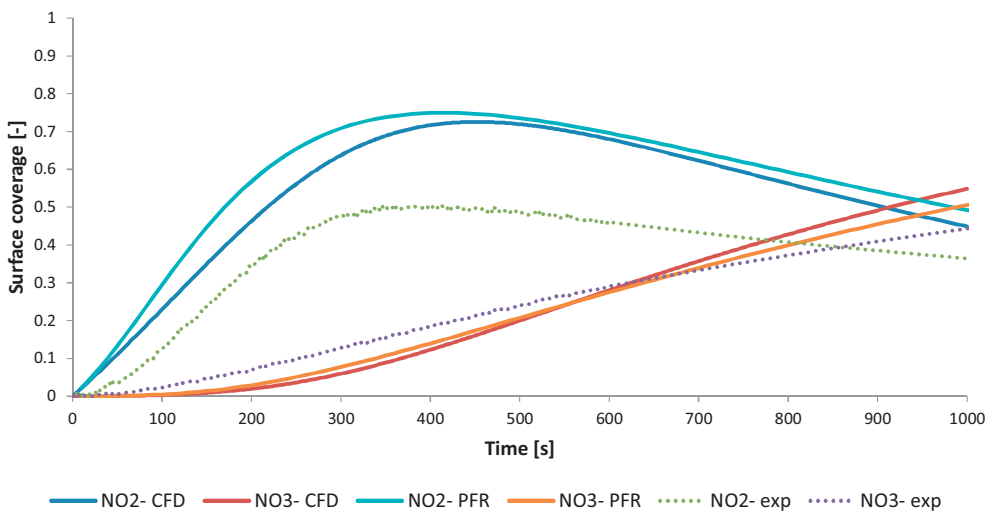

Fig. 9. Surface-averaged coverage of the adspecies on the IR-beam invested area @ 250 °C.

BC:

$$\rho^{C}_{O_2}(t\geq 0,\ \vec{c}\in\partial\wp_{\text{inlet}}) = \frac{0.03\cdot P\cdot MW_{O_2}}{RT} \tag{23}$$

$$\rho^{C}_{NO}(t\geq 0,\ \vec{c}\in\partial\wp_{\text{inlet}}) = \frac{1000[\text{ppm}]\cdot P\cdot MW_{NO}}{RT} \tag{24}$$

$$\rho^{C}_{NO_2}(t\geq 0,\ \vec{c}\in\partial\wp_{\text{inlet}}) = 0 \tag{25}$$

$$\nabla\rho^{C}_{i}(t>0,\ \vec{c}\in\partial\wp_{\text{outlet}}) = 0 \tag{26}$$

$$-\vec{n}_f\cdot\vec{N}^{c}_{i}(t>0,\ \vec{c}\in\partial\wp_{\text{fluid-wall}}) = 0 \tag{27}$$

$$-\vec{n}_f\cdot\vec{N}^{c}_{i}(t>0,\ \vec{c}\in\partial\wp_{\text{solid-wall}}) = R_i MW_i V_{CAT}\frac{A_f}{A_{CAT}} \tag{28}$$

In Eqs. (16)–(28), subscript i refers to gas phase reactants and products (O_2, NO, NO_2), subscript j refers to adspecies (Pt-O, NO_2^-, NO_3^-), while superscript c refers to gas phase cell threads.

The resulting ODE system is composed by approximately 50,000 equations, and is characterized by a diagonally dominant, sparse, Jacobian matrix (Fig. 7). It is possible to highlight the presence of 3 bigger diagonal blocks, which refer to the accumulation and convective terms of the 3 gas phase species (NO, NO_2, O_2), and 3 smaller diagonal blocks, which refer to the adspecies (NO_2^-, NO_3^-, Pt-O). The non-diagonal blocks are related to the reaction term.

3.4.1. CAT-PP simulation results

The time evolution of the concentrations of NO and NO_2 and of the surface coverages of nitrites and nitrates upon stepwise exposure of the catalyst sample to a NO/O_2 mixture at 250 °C is shown in Fig. 8 as representative example of the simulation results. At this temperature, the storage of NO proceeds via a "front mechanism", which results in the complete uptake of NO_x for the first tens of seconds, followed by a progressively breakthrough of NO, which reaches an outlet concentration equal to the inlet concentration around 500s. In the first 300s, NO is stored mainly in the form of nitrites, which are then converted to nitrates starting from the fraction of the catalyst pellet closer to the cell inlet. As a matter of facts, after about 400s, nitrites reach their maximum concentration, while at longer exposure time they are oxidized to nitrates (reaction S5). The latter species, on the contrary, show a monotonic increase with time, with a rate which increases with time as typical of secondary reaction products. Interestingly, simulation results demonstrate that at 250 °C the nitrite route is faster than the nitrate route at the beginning of the NO_x uptake and it leads to the formation of nitrites as precursors in the formation of nitrates: the surface concentration of nitrites is in fact greater than that of nitrates for the first 900s.

3.5. Comparison between CAT-PP and ideal PFR model simulations

The results of the simulation allow to evaluate the extent of the non-idealities of the simulated *operando* FTIR reaction cell. The comparison of the simulation results obtained with the CAT-PP and with the ideal PFR model is provided in Fig. 9, where the experimental data, the results of the simulation with the ideal reactor mode (see Visconti et al., 2013 for more details) and the results of CAT-PP are compared. It is apparent that the ideal PFR and the CAT-PP simulations are in good agreement each other. This proves that the adopted FTIR cell may be described as an ideal reactor or not, thus proving an ex-post validation of the hypothesis done by Visconti et al. (2013) to develop a spectrokinetic model for the NO_x storage over a representative LNT catalyst on the basis of a set of transient surface and gas-phase experimental data collected in such a cell.

Nevertheless, CAT-PP moves toward a better fitting of the experimental data. Such encouraging results demonstrate the possibility to perform CFD simulation of reactive systems with acceptable computational efforts.

4. Conclusion

In this study a numerical methodology was developed to simulate diluted heterogeneous reactive systems basing on a CFD approach. This approach consists of two main steps. At first, a non-reactive CFD simulation is performed using commercial code, and, in a second step, hydrodynamic data are transferred to a post-processor, able to solve the transport equations of the chemical species.

The methodology is considerably adaptable and can handle arbitrary geometries and detailed kinetic schemes. Moreover the simplification assumptions allow to properly model these reactive systems without the compulsory need for a cluster workstation facility.

Its application to the case of the Lean-NO_x-Trap (LNT) lean-phase accumulation demonstrated its numerical viability and effectiveness of prediction with respect to other existing methods.

Comparisons between CAT-PP and ideal PFR models highlight the substantial ideality of the system analyzed, while the first approach could provide further information on the dynamic and spatial behavior of the active surface coverage during the catalyst operation.

The simulator will also be able to investigate different geometries, making possible a sensitivity analysis on the performances of the cell in relation to the geometrical lengths and the position and dimension of the irradiated zone.

Acknowledgments

Authors gratefully acknowledge the insightful discussions with Professor Marco Daturi (Laboratoire Catalyse et Spectrochimie, ENSICAEN, CNRS, Universitè de Caen, 6 Bd du Marèchal Juin, 14050 Caen Cedex, France), Professor Guido Buzzi-Ferraris (Dipartimento di Chimica, Materiali e Ingegneria Chimica "Giulio Natta", Politecnico di Milano – Piazza L. da Vinci, 32 – 20133 Milan, Italy), Professor Sauro Pierucci (Dipartimento di Chimica, Materiali e Ingegneria Chimica "Giulio Natta", Politecnico di Milano – Piazza L. da Vinci, 32 – 20133 Milan, Italy), Professor Luca Lietti (Dipartimento di Energia, Politecnico di Milano – Piazza L. da Vinci, 32 – 20133 Milan, Italy), and Professor Pio Forzatti (Dipartimento di Energia, Politecnico di Milano – Piazza L. da Vinci, 32 – 20133 Milan, Italy).

Appendix.

To support the reader in his/her implementation of CAT-PP methodology, here is reported the UDF used to export the flow field data. As the code is self-consistent, it is simply necessary to copy/paste it in a new c/c++ file and compile and hook the UDF as described in the Fluent Manual.

```
#include "udf.h"
#include "mem.h"
#include "stdio.h"
#include "sg.h"
#include "sg_pdf.h"
#include <string.h>

// ********************************************
//        UDF to generate the input files
// ********************************************

DEFINE_ON_DEMAND(ExportCentroidVariables)
{
FILE *resConn;
FILE *resCell;
FILE *resFace;

Domain *d;
Thread *t;
Thread *tf;
cell_t c;
cell_t c_out;
face_t f;

int n,Nfacce,zone_ID_out;
int righeConn = 0;
int righeCell = 0;
int righeFace = 0;
int i = 0;
double xc[ND_ND];
double xf[ND_ND];
double vol,rho,P,u,v,w,uf,vf,wf;
int zone_ID;

//INTERIOR FACE GEOMETRY
double A[ND_ND];
double ds;
double es[ND_ND];
double A_by_es;
double dr0[ND_ND];
double dr1[ND_ND];

//ADJACENT CELL VARIABLES
double xc_out[ND_ND];
double rho_out,P_out,u_out,v_out,w_out;

d = Get_Domain(1);

resConn = fopen("ExportedConnectivityVariables.txt","w");
resCell = fopen("ExportedCellVariables.txt","w");
resFace = fopen("ExportedFaceVariables.txt","w");
```

```
thread_loop_c(t,d)
{
	begin_c_loop(c,t) // loop over all cells
	{
		zone_ID = THREAD_ID(t); // (velocity-inlet, fluid-wall, ...)
		C_CENTROID(xc,c,t);
		vol = C_VOLUME(c,t);
		rho = C_R(c,t);	// density
		P = C_P(c,t);	// pressure
		u = C_U(c,t);	// u velocity
		v = C_V(c,t);	// v velocity
		w = C_W(c,t);	// w velocity
		Nfacce = C_NFACES(c,t);
		fprintf(resCell,"%e\t%e\t%e\t%e\t%e\t%e\t%e\t%e\n",xc[0],xc[1],xc[2],vol,u,v,w
		,P+101325.);
		fprintf(resConn,"%d\t%d\t%d\t%d\t%d\t%d\n",zone_ID,c+1,Nfacce,0,0,0);
		righeConn = righeConn + 1;
		righeCell = righeCell + 1;
		c_face_loop(c,t,n) // loop over all faces of the cell
		{
			righeConn = righeConn + 1;
			f = C_FACE(c,t,n);
			tf = C_FACE_THREAD(c,t,n);
			zone_ID = THREAD_ID(tf);
			if(BOUNDARY_FACE_THREAD_P(tf)) // faces on the boundary
			{
				// CELL
				int solid_wall = 7;
				if(THREAD_ID(tf) == solid_wall)
				{
					i = i + 1;
					fprintf(resConn,"%d\t%d\t%d\t%d\t%d\t%d\n",zone_ID,f+1,i,0
					,0,0);
				}
				else
				{
					fprintf(resConn,"%d\t%d\t%d\t%d\t%d\t%d\n",zone_ID,f+1,0,0
					,0,0);
				}
			}
			else	// internal faces
			{
				// ADJACENT CELL
				if(c==F_C0(f,tf)) //the adjacent cell is on the boundary side
				{
					c_out = F_C1(f,tf);
					zone_ID_out = THREAD_ID(THREAD_T1(tf));
					fprintf(resConn,"%d\t%d\t%d\t%d\t%d\t%d\n",zone_ID,f+1,0,z
					one_ID_out,c_out+1,0);
					// 0: A has a normal vector direction exiting from the
					cell
				}
				else if(c==F_C1(f,tf))//the adjacent cell is on the interior side
				{
					c_out = F_C0(f,tf);
					zone_ID_out = THREAD_ID(THREAD_T0(tf));
					fprintf(resConn,"%d\t%d\t%d\t%d\t%d\t%d\n",zone_ID,f+1,0,z
					one_ID_out,c_out+1,1);
					// 1: A has a normal vector direction entering in the cell
				}
			}
		}
	}
```

```
        end_c_loop(c,t)
}
// FACE DATABASE
thread_loop_f(tf,d)
{
        if(THREAD_ID(tf) != 8 && THREAD_ID(tf) != 9 && THREAD_ID(tf) != 10)
        {
                begin_f_loop(f,tf)
                {
                        zone_ID = THREAD_ID(tf);
                        F_CENTROID(xf,f,tf);
                        righeFace = righeFace + 1;
                        if(BOUNDARY_FACE_THREAD_P(tf)) // face on the boundary
                        {
                                BOUNDARY_FACE_GEOMETRY(f,tf,A,ds,es,A_by_es,dr0);
                                uf = F_U(f,tf);
                                vf = F_V(f,tf);
                                wf = F_W(f,tf);
                                fprintf(resFace,"%e\t%e\t%e\t%e\t%e\t%e\n",A[0],A[1],A[2],uf,vf,w
                                f);
                        }
                        else // internal face
                        {
                                INTERIOR_FACE_GEOMETRY(f,tf,A,ds,es,A_by_es,dr0,dr1);
                                fprintf(resFace,"%e\t%e\t%e\t%e\t%e\t%e\n",A[0],A[1],A[2],xf[0],x
                                f[1],xf[2]);
                        }
                }
                end_f_loop(f, tf)
        }
}

fprintf(resConn,"%d\t%d\n",righeConn,6);
fprintf(resFace,"%d\t%d\n",righeFace,6);
fprintf(resCell,"%d\t%d\n",righeCell,8);
fclose(resConn);
fclose(resCell);
fclose(resFace);
}
```

References

ANSYS. (2009). *ANSYS FLUENT 12. 0: UDF Manual*.

Benjamin, S. F., & Roberts, C. A. (2007). Three-dimensional modelling of NO_x and particulate traps using CFD: A porous medium approach. *Applied Mathematical Modelling*, *31*, 2446–2460.

Buzzi-Ferraris, G., & Manenti, F. (2012). BzzMath: Library overview and recent advances in numerical methods. *Computer Aided Chemical Engineering*, *30*, 1312–1316.

Carias-Henriquez, A., Pietrzyk, S., & Dujardin, C. (2013). Modelling and optimization of IR cell devoted to in situ and operando characterization of catalysts. *Catalysis Today*, *205*, 134–140.

Centi, G., Ciambelli, P., Perathoner, S., & Russo, P. (2002). Environmental catalysis: trends and outlook. *Catalysis Today*, *75*, 3–15.

Corbetta, M., Manenti, F., Visconti, C. G., Pierucci, S., Lietti, L., & Forzatti, P. (2013). Development of a kinetic model of lean-NO_x-trap and validation through a reactive CFD approach. *Chemical Engineering Transactions*, *32*, 643–648.

Deutschmann, O. (2001). *Interactions between transport and chemistry in catalytic reactors*. Unpublished Habilitation: Ruprecht-Karls-University of Heidelberg (thesis).

Durand, G., Manenti, F., Bandoni, J. A., Diaz, M. S., & Buzzi-Ferraris, G. (2012). Performance assessment of existing methodologies for chemical process dynamic simulation. *Chemical Engineering Transactions*, *29*, 241–246.

European Parliament, E. (2007). *Regulation (EC) No 715/2007 of the European Parliament and of the Council of 20 June 2007 type approval of motor vehicles with respect to emissions from light passenger and commercial vehicles (Euro 5 and Euro 6) and on access to vehicle repair and maintenance information*.

Kolaczkowski, S. T., Chao, R., Awdry, S., & Smith, A. (2007). Application of a CFD code (FLUENT) to formulate models of catalytic gas phase reactions in porous catalyst pellets. *Chemical Engineering Research & Design*, *85*, 1539–1552.

Lietti, L., Daturi, M., Blasin-Aube, V., Ghiotti, G., Prinetto, F., & Forzatti, P. (2012). Relevance of the nitrite route in the NO_x adsorption mechanism over Pt-Ba/Al_2O_3 NO_x storage reduction catalysts investigated by using operando FTIR spectroscopy. *Chemcatchem*, *4*, 55–58.

Maestri, M., & Cuoci, A. (2013). Coupling CFD with detailed microkinetic modeling in heterogeneous catalysis. *Chemical Engineering Science*, *96*, 106–117.

Manenti, F. (2011). Considerations on nonlinear model predictive control techniques. *Computers & Chemical Engineering*, *35*, 2491–2509.

Manenti, F., Cieri, S., Restelli, M., & Bozzano, G. (2013). Dynamic modelling of the methanol synthesis fixed-bed reactor. *Computers & Chemical Engineering*, *48*, 325–334.

Meunier, F. C. (2010). The design and testing of kinetically-appropriate operando spectroscopic cells for investigating heterogeneous catalytic reactions. *Chemical Society Reviews*, *39*, 4602–4614.

Nova, I., Castoldi, L., Lietti, L., Tronconi, E., Forzatti, P., Prinetto, F., & Ghiotti, G. (2004). NO_x adsorption study over Pt-Ba/alumina catalysts: FT-IR and pulse experiments. *Journal of Catalysis*, *222*, 377–388.

Stepanek, J., Koci, P., Marek, M., & Kubicek, M. (2012). Catalyst simulations based on coupling of 3D CFD tool with effective 1D channel models. *Catalysis Today*, *188*, 87–93.

Visconti, C. G., Lietti, L., Manenti, F., Daturi, M., Corbetta, M., Pierucci, S., & Forzatti, P. (2013). Spectrokinetic analysis of the NO_x storage over a Pt-Ba/Al_2O_3 Lean NO_x trap catalyst. *Topics in Catalysis*, 1–6.

Visconti, C. G., Tronconi, E., Lietti, L., Forzatti, P., Rossini, S., & Zennaro, R. (2011). Detailed kinetics of the Fischer–Tropsch synthesis on cobalt catalysts based on H-assisted CO activation. *Topics in Catalysis*, *54*, 786–800.